Ocean Engineering 59 (2013) 1–8

Contents lists available at SciVerse ScienceDirect

Ocean Engineering

journal homepage: www.elsevier.com/locate/oceaneng

Neuro-fuzzy based approach for estimation of Hydrofoil performance

M.H. Djavareshkian *, A. Esmaeili

Ferdowsi University of Mashhad, Iran

ARTICLE INFO

Article history:
Received 18 February 2011
Accepted 27 October 2012

Keywords:
ANFIS
Hydrofoil
Estimation
Hydrodynamic
Performance

ABSTRACT

In this research, a numerical procedure is used to solve the Navier-Stokes equation on a submerge hydrofoil and the estimation of hydrofoil performance is done by an Adaptive Neuro-Fuzzy Inference System (ANFIS) model. A pressure-based implicit technique and a non-orthogonal mesh with collocated finite volume formulation are used to simulate flow around the hydrofoil. The procedure incorporates the $k-\varepsilon$ eddy-viscosity turbulence model and a Volume of Fluid (VOF) process has been utilized to simulate two-phase fluid (water and air). In the mentioned method, the analyses of thickness and camber effect of hydrofoil, submerge distance (h/c), and the angle of attack (AOA) make an impression on the hydrofoil performance. To verify the numerical simulation, a part of the presented results is compared with the published experimental data. This comparison confirms the numerical process. Moreover, the hydrofoil configuration and operating condition are assessed by ANFIS model. Consequently, the results prove that the ANFIS model can predicate the hydrofoil performance very well.

1. Introduction

The estimation of hydrofoil performance and finding a mathematical model play a significant role in many engineering applications, particularly in marine vehicles. The hydrofoil is widely used in marine vehicles and it increases the speed of vehicles, maneuverability, stability and performance of the vehicles, but hydrofoil performance depends on other parameters as the camber of hydrofoil, submerge distance, and the angle of attack and the thickness of hydrofoil. In addition, this performance affects on wave generation on free surface. Therefore, an accurate estimation of hydrofoil performance for a safe and economical design of a marine has to be considered, so that it can reduce energy consumption in operating conditions. There is a great volume of published work dealing with moving hydrofoil performances (De Blasi et al., 2000; Daskovsky, 2000; Filippov, 2001; Rhee et al., 2003; Bourgoyne, 2003; Hay and Visonneau, 2005; Chen and Liu, 2005; Antonio et al., 2005; Kouh et al., 2002). But it is noticed that there is a lake of a simple mathematical model to predict submerge hydrofoil performance, which moved near the free surface of water. Although a number of studies has been carried out considering a floating hydrofoil with some assumptions common in hydrodynamics, which proves less improvement.

In the last decades, extensive studies have been carried out on the hydrofoil (Xie and Vassalos, 2007; Sadathosseini et al., 2008; Antoine et al., 2009). Another point that should be considered is the control system of marine transport. The current control system of a fully submerged hydro-craft has manual input. However, the manual input depends on human individual skills and the observation of waves encountering the work well over a wide range of waves, while if the wave profile has been estimated, the best system performance can be well estimated. For finding a good estimation of the wave profile, it needs to predict hydrofoil treatment (Kim and Yamato, 2005) and finding a mathematical model.

In the recent years, the research interest in artificial neural network has increased and many efforts have been made on application of neural networks to various marine engineering problems. Many researchers have developed a hybrid model by mixture the neural network with fuzzy logic to solve ocean engineering problems (Kazeminezhad et al., 2005; Bateni and Jeng, 2007; Guven et al., 2009). Futhermore, Patil et al. (in press) have investigated the performance of Neuro-Fuzzy method for predicting wave transmission coefficient of horizontally interlaced multilayer moored floating pipe breakwater. However, it is observed that there are hardly any applications of soft computing tools on the estimation of floating hydrofoil performance, moved near the free surface of water.

In the present paper, floating hydrofoil performance and the estimation of wave generation on the free surface have been investigated by ANFIS, while this technique is more flexible then other approach. In this research, the type of hydrofoil (camber and thickness), submerge distance (h/c) and the angle of attack (AOA) have been impressed on wave profile and hydrofoil performance.

* Corresponding author. Tel./fax: +98 5118763304.
E-mail addresses: javareshkian@ferdowsi.um.ac.ir (M.H. Djavareshkian), aliesmaeli30316@yahoo.com (A. Esmaeili).

0029-8018/$ - see front matter © 2012 Elsevier Ltd. All rights reserved.
http://dx.doi.org/10.1016/j.oceaneng.2012.10.015

The novelty of this study is the investigation of ANFIS model in the prediction of hydrofoil performance according to its configuration and operating conditions. It is possible to evaluate the relative importance of input parameters on the moving submerge hydrofoil on the water. The results are tabulated in terms of statistical measures, and they are demonstrated in scatter plans.

2. Theoretical routines

2.1. Adaptive Neuro-fuzzy inference system (ANFIS) architecture

Artificial neural network is a favorable technique to solve optimization problems, because it can simulate the operations of the brain and uses parallel processing to save computational time. Fuzzy logic approach is another intelligent computing tool, which is competent for applying to wide variety of problems. Neural Networks (NN) are demonstrated to have powerful capability of expressing relationship between input–output variables. Recently, there has been a growing interest in combining both these approaches, and as a result, Neuro-Fuzzy computing techniques have been evolved. These are fuzzy systems, which use neural networks theory in order to determine their properties (fuzzy sets and fuzzy rules) by processing data samples (Mitra and Hayashi, 2002). Neuro-Fuzzy integrates to synthesize the merits of both neural networks and fuzzy systems in a complementary way to overcome their disadvantages. ANFIS model has combined the neural network adaptive capabilities and the fuzzy logic qualitative approach which Jang (1993) has presented. The mentioned model has been attained its popularity due to a broad range of useful applications in such diverse areas in recent years as optimization of fishing predictions (Nuno et al., 2005; Noureldin et al., 2007; Kishor et al., 2007; Lee and Gardner, 2006; Übeyli and Güler, 2006; Civicioglu, 2007; Qin and Yang, 2007; Daoming and Jie, 2006; Depari et al., 2006; Assaleh, 2007; Huang et al., 2007).

All above works manifest that ANFIS model is considered as a good universal approximation, predictor, interpolator and estimator. They demonstrate that each non-linear function of many inputs and outputs can be easily constructed with the model. A typical architecture of the model is illustrated in Fig. 1, in which a circle indicates a fixed node, and a square depicts an adaptive node. For simplicity, two inputs x, y and one output z in the fuzzy inference system (FIS) can be considered. The ANFIS in this paper implements a Sugeno-Fuzzy type inference system. For example, for a Sugeno-Fuzzy model, a common rule set with two fuzzy if-then rules can be expressed as:

Rule 1: If x is A1 and y is B1,

Then

$$z_1 = p_1x+q_1y+r_1 \tag{1}$$

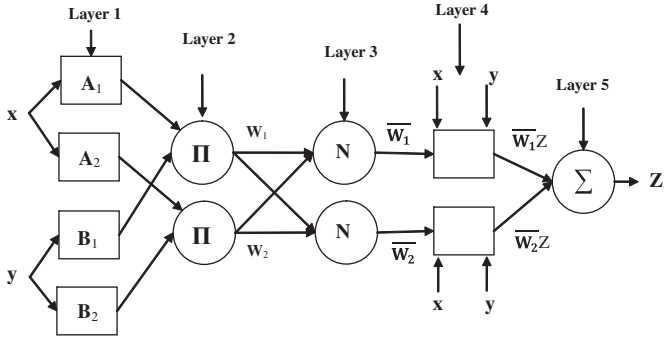

Fig. 1. ANFIS architecture Π, N, Σ are defined in Eqs. (20), (21), (23), respectively.

Rule 2: If x is A2 and y is B2,

Then

$$z_2 = p_2x+q_2y+r_2 \tag{2}$$

where A_i, B_i $(i=1,2)$ A_i and B_i are fuzzy sets in the antecedent, and p_i,q_i,r_i $(i=1,2)$ are the design parameters that are determined during the training process.

As in Fig. 1, the ANFIS consists of five layers:

Layer 1, every node i in this layer is an adaptive node with a node function:

$$\begin{aligned} O_i^1 &= \mu_{A_i}(x), \quad i=1,2 \\ O_i^1 &= \mu_{B_i}(y), \quad i=1,2 \end{aligned} \tag{3}$$

where x,y are the input of node i, and $\mu_{A_i}(x)$ and $\mu_{B_i}(y)$ can adopt any fuzzy membership function (MF). In this paper, Gaussian MFs are used:

$$\text{gaussian}\,(x,c,\sigma) = e^{-(1/2)(x-c/\sigma)^2} \tag{4}$$

where c is center of Gaussian MF and σ is a standard deviation of this cluster. In layer 2, every node represents the ring strength of a rule by multiplying the incoming signals and forwarding the product as:

$$O_i^2 = \omega_i = \mu_{A_i}(x)\mu_{B_i}(y), \quad i=1,2 \tag{5}$$

In layer 3, the ith node calculates the ratio of the ith rules ring strength to the sum of all rules ring strengths:

$$O_i^3 = \varpi_i = \frac{\omega_i}{\omega_1+\omega_2}, \quad i=1,2 \tag{6}$$

where ϖ_i is referred to as the normalized ring strengths.

In layer 4, the node function is represented by

$$O_i^4 = \varpi_i z_i = \varpi_i(p_ix+q_iy+r_i), \quad i=1,2 \tag{7}$$

where ϖ_i is the output of layer 3, and $\{p_i,q_i,r_i\}$ are the parameter set which are referred to as the consequent parameters.

In layer 5, the single node computes the overall output as the summation of all incoming signals:

$$O_i^5 = \sum_{i-1}^{2} \varpi_i z_i = \frac{\omega_1 z_1+\omega_2 z_2}{\omega_1+\omega_2} \tag{8}$$

It is clear that the ANFIS has two sets of adjustable parameters, namely the premise and consequent parameters. During the learning process, the premise parameters in the first layer and the consequent parameters in the fourth layer are tuned until the desired response of the FIS is achieved. In this work, the Hybrid learning algorithm (Jang et al., 2002), which combines the Least Square method (LS) and the back propagation (BP) algorithm, is utilized to rapidly train and adapt the FIS. When the premise parameter values of the membership function are fixed, the output of the ANFIS can be written as a linear combination of the consequent parameters:

$$z = (\varpi_1 x)p_1+(\varpi_1 x)q_1+(\varpi_1)r_1+(\varpi_2 x)p_2+(\varpi_2 x)q_2+(\varpi_2)r_2 \tag{9}$$

The LS method can be applied to determine optimally the values of the consequent parameters. When the premise parameters are not fixed, the search space becomes larger and the convergence of training becomes slower. The Hybrid algorithm converges much faster since it reduces the dimension of the search space of the BP algorithm. During the learning process, the premise parameters in layer 1 and the consequent parameters in layer 4 are tuned until the desired response of the FIS is achieved. The hybrid-learning algorithm has a two-step process. First, while holding the premise parameters fixed, the functional signals are propagated forward to layer 4, where the consequent parameters are identified by the least square method. Second, the consequent

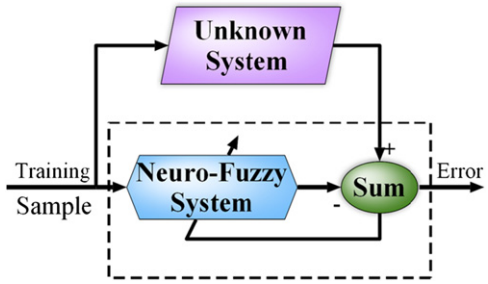

Fig. 2. Process of ANFIS.

parameters are held fixed while the error signals, the derivative of the error measure with respect to each node output, are propagated from the output end to the input end, and the standard BP algorithm updates the premise parameters.

Fig. 2 demonstrates a schematic of the model, which the input data is repeatedly presented. With each presentation, the output of the model is compared with the desired output and an error is computed. This error is fed back (back propagated) to the ANFIS and it is utilized to adjust the weights so that the error is decreased by each iteration and the neural model gets closer and closer to produce the desired output. This process is known as "Training". The approach utilizes this error to adjust its weights in order to decrease the error and this sequence of events is usually repeated until either an acceptable error has been reached or the no longer network has been appeared to be learning.

2.2. Convergence Criteria for estimation

The performance efficiency of the network is evaluated by comparing the numerical values with the approach-estimated ones. In addition to MSE (Mean Squared Error), NMSE (Normalized Mean Squared Error), MAE (Mean Absolute Error) and R^2 (coefficient of determination) are applied as the other parameters for the calculation of error in this modeling (Eqs. (10)–(14)). In brief, this technique prediction is optimum if R^2, MAE, NMSE and MSE are found to be close to 1, 0, 0 and 0, respectively.

$$MSE = \frac{\sum_{i=1}^{N}(O_i - T_i)^2}{N} \tag{10}$$

$$NMSE = \frac{1}{\sigma^2}\frac{1}{N}\sum_{i=1}^{N}(O_i - T_i)^2 \tag{11}$$

$$MAE = \sum_{i=1}^{N}\frac{(O_i - T_i)}{N} \tag{12}$$

$$R^2 = 1 - \frac{\sum_{i=1}^{N}(O_i - T_i)^2}{\sum_{i=1}^{N}(O_i - T_m)^2} \tag{13}$$

$$T_m = \frac{\sum_{i=1}^{N} O_i}{N} \tag{14}$$

where O_i is the i^{th} numerical value, T_i is the i^{th} predicted value, N is the number of data and σ^2 is the variance of numerical data.

2.3. Numerical solution process

The basic equations, which describe conservation of mass, momentum and scalar quantities, can be expressed in the following vector form, which is independent of the coordinate system.

$$\frac{\delta\rho}{\delta t} + div\left(\rho\vec{V}\right) = S_m \tag{15}$$

$$\frac{\delta\left(\rho\vec{V}\right)}{\delta t} + div\left(\rho\vec{V}\otimes\vec{V} - \vec{T}\right) = \vec{S}_v \tag{16}$$

$$\frac{\delta(\rho\phi)}{\delta t} + div\left(\rho\vec{V}\phi - \vec{q}\right) = \vec{S}_\phi \tag{17}$$

Where ρ, $\vec{V}$ and ϕ are density, velocity vector and scalar quantity respectively, $\vec{T}$ is the stress tensor and $\vec{q}$ is the scalar flux vector. The latter two are usually expressed in terms of basic dependent variables. The stress tensor for a Newtonian fluid is

$$\vec{T} = -P\vec{I} \tag{18}$$

and the Fourier-type law usually gives the scalar flux vector:

$$\vec{q} = \Gamma_\phi grad\phi \tag{19}$$

In this study, $k-\varepsilon$ model is used for turbulence flow. The discretization of the above differential equations is carried out by applying a finite-volume approach. First, the solution domain is divided into a finite number of discrete volumes or cells, where all variables are stored at their geometric centers. The equations are then integrated over all the control volumes by utilizing the Gaussian theorem. The discrete expressions are presented to refer to only one face of the control volume, namely, e, for the sake of brevity. For any variable ϕ (which may also stand for the velocity components), the result of the integration yields:

$$\frac{\delta v}{\delta t}\left[(\rho\phi)_p^{n+1} - (\rho\phi)_p^n\right] + I_e - I_w + I_n - I_s = S_\phi \delta v \tag{20}$$

where, I's are the combined cell-face convection I^c and diffusion I^D fluxes. The diffusion flux is approximated by central differences. The discretization of the convective flux requires special attention and it causes to develop the various schemes. A representation of the convective flux for cell-face (e) is:

$$I_e^c = (\rho.V.A)_e\phi_e = F_e\phi_e \tag{21}$$

The value of ϕ_e is not known and should be estimated from the values at neighboring grid points by interpolation. The expression for the ϕ_e is determined by Second order Upwind scheme. The final form of the discretized equation from each approximation is given as:

$$A_p\phi_p = \sum_{m=E,W,N,S} A_m\phi_m + S_\phi' \tag{22}$$

Where A's are the convection-diffusion coefficients. The term S_ϕ' in Eq. (22) contains quantities arising from non-orthogonality, numerical dissipation terms and external sources. For the momentum equations, it is easy to separate out the pressure-gradient source from the convection momentum fluxes.

VOF ideas have been utilized to simulate two-phase fluid (water and air). The VOF model can model two or more immiscible fluids by solving a single set of momentum equations and tracking the volume fraction of each of the fluids throughout the domain. The tracking of the interface between the phases is accomplished by the solution of a continuity equation for the volume fraction of one of the phases. For the qth phase, this equation has the following form:

$$\frac{1}{\rho}\left[\nabla.\left(\alpha_q\rho_q\vec{v}\right) = S_{pq} + \sum_{p=1}^{n}\left(\dot{m}_{pq} - \dot{m}_{qp}\right)\right] \tag{23}$$

where $\dot{m}_{pq}$is the mass transfer from phase q to phase p, and $\dot{m}_{qp}$is the mass transfer from phase p to phase q. S_{pq} is the source term which in this problem is zero. The volume fraction equation will not be solved for the primary phase. The primary-phase volume

fraction will be computed based on the following constraint:

$$\sum_{q=1}^{n} \alpha_q = 1 \tag{24}$$

The volume fraction equation may be solved either through implicit or explicit discretization. In this research, implicit is used.

3. Results

3.1. Computation simulation output

The data sets used in this study are achieved from Computational Fluid Dynamic (CFD) laboratory and they include numerical simulation. In the numerical simulation, grid, domain independency, and comparison with currant result and published data should be investigated. The grid structure in CFD simulation is created by a structured mesh. In this simulation, H-type grid is used and boundary condition is illustrated in Fig. 3. At the inlet, velocity is prescribed. At the outlet, the pressure is fixed. Slip boundary conditions are utilized on upper walls of the domain and wall boundary conditions are applied for hydrofoil surface.

According to Fig. 3, the dimension of domain has been obtained by doing several various lengths and independent lengths have been selected. The grid sizing is determined after grid independence that is found by doing several different trials which demonstrate surface pressure coefficient distribution at hydrofoil with NACA4412 area section, AOA=5°, h/c=1 and Fc=1. The effect of grid size is illustrated in Fig. 4. For other cases, the above process is utilized for grid and domain independences.

In this study, the Froude number (Fc) is equal 1 (according to the chord of hydrofoil). The setting of numerical simulation has been confirmed in Table 1.

To validate the numerical simulation, lift coefficient of NACA4412 hydrofoil is compared with the experimental data (Kouh et al., 2002). Fig. 5 indicates the lift coefficient of hydrofoil NACA4412 for an AOA=5° and h/c=1. Comparisons demonstrate that the numerical results are in a good agreement with experimental data.

In this research, the effect of the camber and thickness of the hydrofoil has numerically been investigated in different angle of attack and various submerge distances. However, the lift and drag coefficients and lift to drag ratio have been analyzed at three special angles of attack 2.5°, 5° and 7.5° degrees; moreover, the submerge distance in the study falls into three main categories: h/c=0.5, 0.7 and 1. Besides, to attain the best mathematical modeling of floating hydrofoil performance, the camber and thickness of hydrofoils should be taken into consideration; therefore, a broad range of them are designated and both of them are divided into three segments. The non-dimensional camber is slightly changed from 0c to 0.02c and 0.04c; also, the non-dimensional thickness is gently varied from 0.09c to 0.12c and 0.15c. For example, the hydrodynamic characteristics of five different 2D hydrofoils, NACA0012, 2412, 4412, 4409, and 4415, are examined according to assumed cambers and thicknesses. Table 2(a)–(e) represents the lift and drag coefficients and L/D in the variant angles of attack as varying submerge distances. Indeed, the tables demonstrate some significant trends; for instance, the lift has an downward trend for all cases when the hydrofoils approach closely to the free surface of water. In almost all of the cases, the lift coefficients are dramatically risen by a gradual growth of the camber and also a slight drop of the thickness. The same is true for drag coefficients (Djavareshkian et al., 2010).

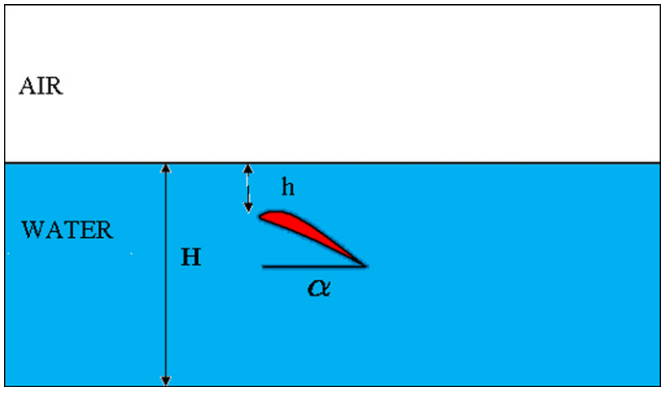

Fig. 3. Dimension and boundary condition of 2D domain.

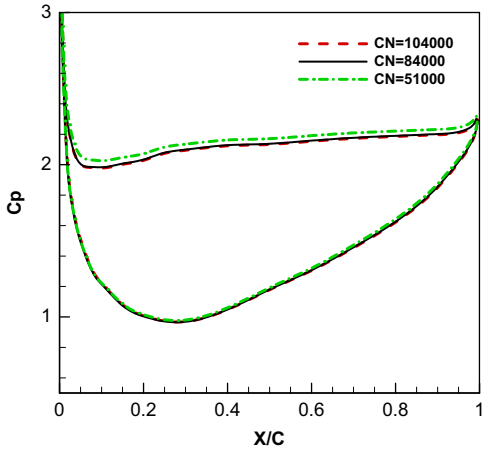

Fig. 4. Effect of grid sizing on pressure distribution on the surface of the NACA4412 hydrofoil for an AOA=5° a, Fc=1 and h/c=1.

Table 1
Settings for numerical simulation.

Flow	Turbulent
Solver	2-D double precision
Momentum equation solver	Second order upwind
Solver	SIMPLE
Turbulent model	$k-\varepsilon$

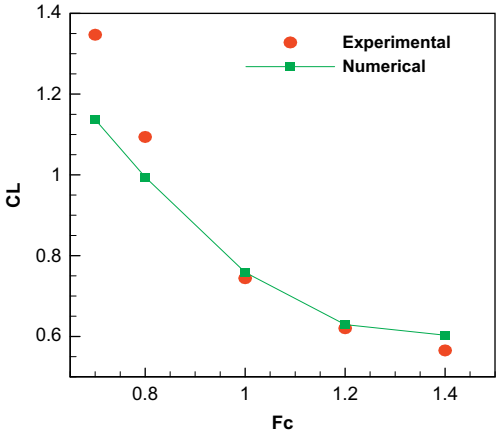

Fig. 5. Comparison of lift coefficient for numerical and experimental data for NACA4412, AOA=5° and h/c=1.

3.2. Estimation process

After numerical simulation, the data are obtained, but they are like a point in the search space. These data are not continuous and they have a nonlinear behavior. Nonlinear system identification is becoming an important tool, which can be achieved by robust fault-tolerant behavior. The data have a nonlinear behavior and the type of system that is between input and output variables is not known. Therefore, ANFIS model is utilized to know the system. In this modeling, the camber, the thickness, the angle of attack and the submerge distance are used as an input and lift to drag (L/D) ratio is utilized as an output. In order to model L/D, a computer program is performed under MATLAB (version 7.7. The Math Works Inc., USA) environment by applying the ANFIS toolbox. A hybrid-learning algorithm is utilized for the model training, and the number of epochs is elected as 100. For the generation, sub clustering is applied, and the parameters for clustering genfis are in Table 3. The number of the membership function is 2 for each input and the total rules are 16, $(2\times2\times2\times2)$, respectively. The type of the membership function is "gaussmf" and it is symmetrical function. For instance, Fig. 6 demonstrates membership function for camber/c.

The total number of data acquired at the time of this study is added up to 81, which have been collected by performing the same different sampler. To introduce the database to the model, it needs to be randomly broken down into two groups: training and testing. This new approach is trained by using the training set data and the test set is utilized to evaluate the predictive ability of the ANFIS. The training is continued as long as the computed error between the actual and predicted outputs for the test set is decreased. Typically, 74% of the data are applied for training and the rest are categorized as testing. The testing set is used to evaluate the accuracy of the newly trained ANFIS by providing the mentioned model a set of data, which have been never considered, before. During the testing, the learning is turned off and the chosen data set is fed through the model. The model output

Table 2
Lift and drag coefficients and L/D ratio of hydrofoils (a) NACA0012, (b) NACA2412, (c) NACA4412, (d) NACA4409, and (e) NACA4415.

AOA (deg)	h/c					
	0.5		0.7		1	
	CL	CD	CL	CD	CL	CD
2.5	0.152	0.0593	0.213	0.0622	0.285	0.0642
5	0.294	0.0727	0.377	0.0783	0.477	0.0826
7.5	0.421	0.0942	0.537	0.1048	0.667	0.1131
(a)						
2.5	0.235	0.0659	0.314	0.0699	0.418	0.0720
5	0.374	0.0807	0.480	0.0879	0.620	0.0929
7.5	0.509	0.1048	0.646	0.1170	0.807	0.1255
(b)						
2.5	0.332	0.0823	0.447	0.0884	0.572	0.0892
5	0.472	0.0992	0.622	0.1099	0.758	0.1133
7.5	0.613	0.1259	0.776	0.1408	0.981	0.1504
(c)						
2.5	0.339	0.0685	0.435	0.0729	0.570	0.0738
5	0.483	0.0867	0.614	0.0951	0.779	0.0993
7.5	0.630	0.1154	0.784	0.1285	0.985	0.1379
(d)						
2.5	0.341	0.0989	0.455	0.1061	0.597	0.1087
5	0.485	0.1160	0.601	0.1261	0.788	0.1316
7.5	0.620	0.1435	0.782	0.1589	0.995	0.1689
(e)						

Table 3
Parameter for clustering genfis.

Range of influence	1
Squash factor	2
Accept ratio	0.5
Reject ratio	0.15

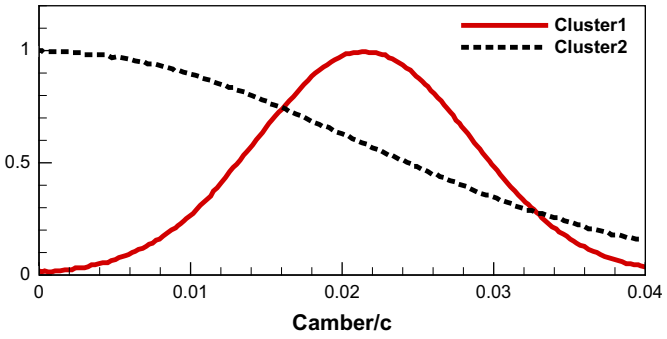

Fig. 6. Membership function for camber/c.

Table4
ANFIS performance values for train and test.

	MSE	NMSE	MAE	R^2
Train	0.021	0.0135	0.1091	0.9867
Test	0.0351	0.0298	0.1487	0.9732

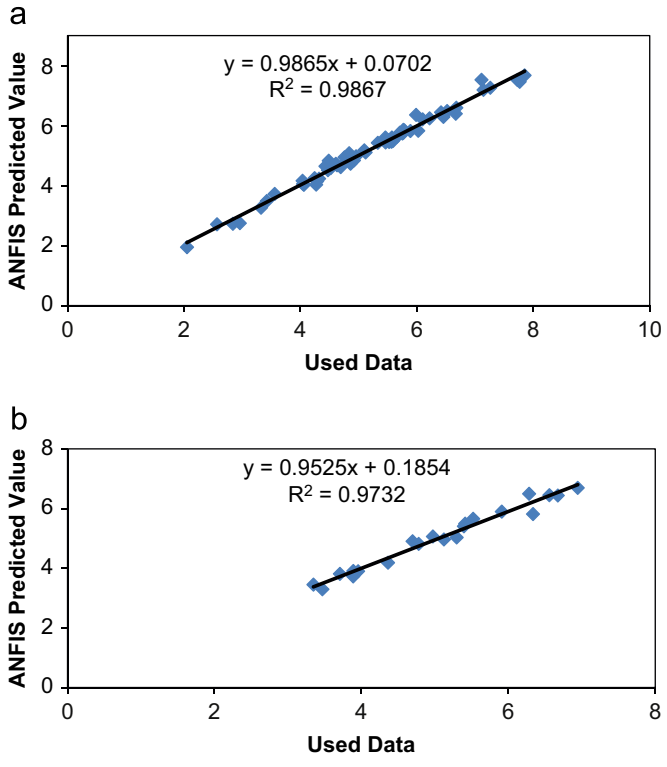

Fig. 7. Numerical results versus ANFIS predicted values of L/D: (a) training data, and (b) testing data.

is collected and a report is then generated for confirming the testing results.

The efficiency of this approach is evaluated whenever the L/D measured values and estimated ANFIS ones are compared. Table 4 illustrates the method performance in the terms of MSE, NMSE, MAE and the coefficient of determination R^2. The low value of the sundry error types especially NMSE and high amount of R^2 particularly in train. Consequently, the results of the test errors reveal the accuracy of the model.

In Fig. 7a and b, the prediction values versus numerical ones of L/D are depicted in the training and testing sets. As a result of these figures, the coefficient of determination is found to be 0.9867 in training and 0.97332 in testing set, where both are well close to 1. The superior agreement between numerical data and the prediction results indicates that it can be used as a powerful method for the prediction of L/D.

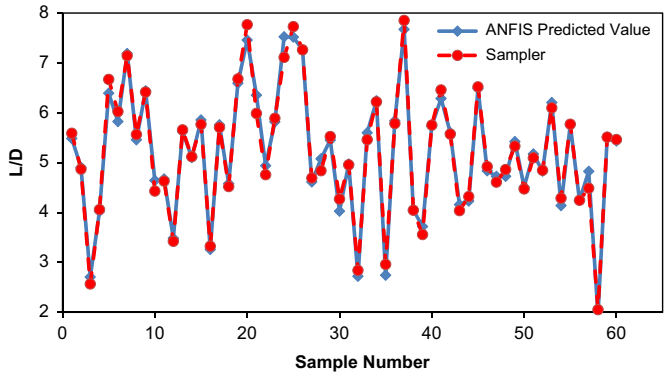

Fig. 8. Comparison of the ANFIS predicted and numerical values of lift to drag ratio in train.

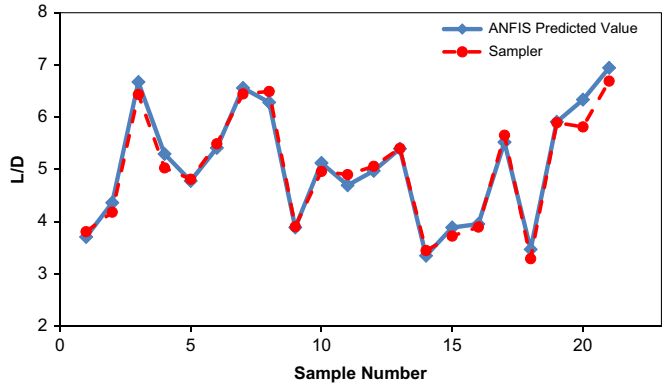

Fig. 9. Comparison of ANFIS prediction and numerical results of lift to drag ratio in test.

The numerical and prediction lift to drag ratio values of the training and testing data sets are illustrated in Figs.8 and 9. As it can be observed in Fig. 8, the lines representing the CFD values and the results estimated by the ANFIS are so close that they are indistinguishable in training. Fig. 9 illustrates the assessment of trained system with 21 data. It is obvious that prediction lift to drag ratio by using this model and numerical values are found in a perfect match in the testing data and there is no recognizable deviation.

As it is known, either humans or other computer techniques can utilize ANFIS, with its significant ability to derive meaning from complicated data, to extract patterns and detect trends that are too complex to be noticed.

Figs. 10–12 demonstrate the 3D plots of the model obtained from ANFIS by using training data. In these modeled figures, lift to drag ratio is plotted versus camber, thickness, the angle of attack and submerge distance. To illustrate the accuracy of the obtained model, L/D numerical values are depicted versus different parameters on the 3D model. Considering these figures, it is obvious that the model surfaces close to the numerical data, appropriately.

Fig. 10 shows L/D ratio versus AOA and camber. It can be seen that increasing AOA causes L/D ratio to grow. This treatment is well estimated by the new approach. In addition, the high value of the camber increases L/D ratio in the large AOA.

Fig. 12 illustrates the effect of submerge distance (h/c) and the thickness effect. The effect of h/c surges towards a straight line, so the rising of h/c causes an increase in L/D ratio. The figure confirms that pressure on the upper surface of hydrofoil is changed more by enhancing h/c. Also, Fig. 12 shows the effect of hydrofoil thickness on L/D ratio and it can be observed that escalating thickness leads to decline in the L/D ratio. When the thickness of hydrofoil becomes more, drag coefficient is picked up and consequently the L/D ratio is mounted. Hence, this model is very strong and it predictes physical treadment, very well.

4. Conclusion

Prediction of hydrofoil performance and free surface wave generation are necessary in order to design a marine engineering. Researchers have carried out tremendous work dealing with

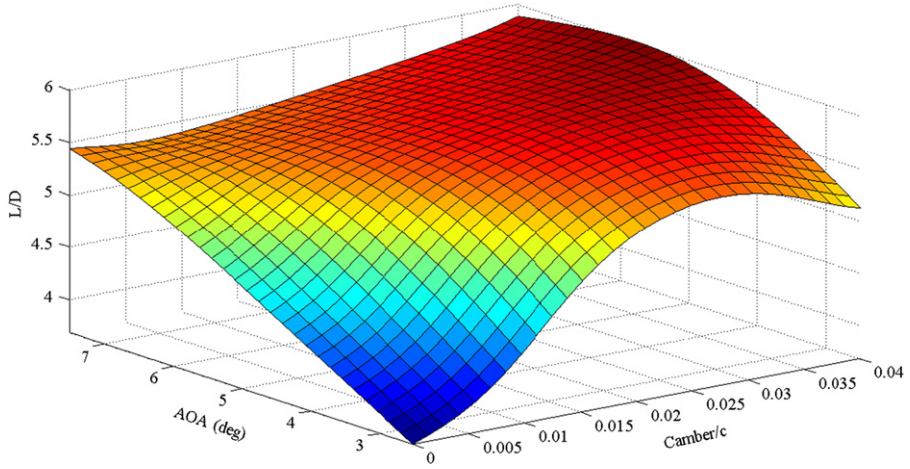

Fig. 10. Generalization of best-fitted surfaces predicted with ANFIS based camber/c, AOA and L/D.

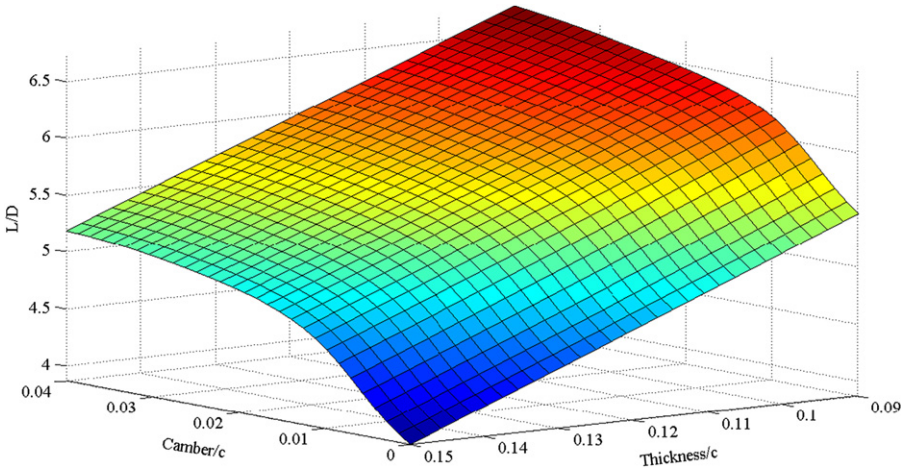

Fig. 11. Generalization of best-fitted surfaces predicted with ANFIS based camber/c, thickness/c and L/D.

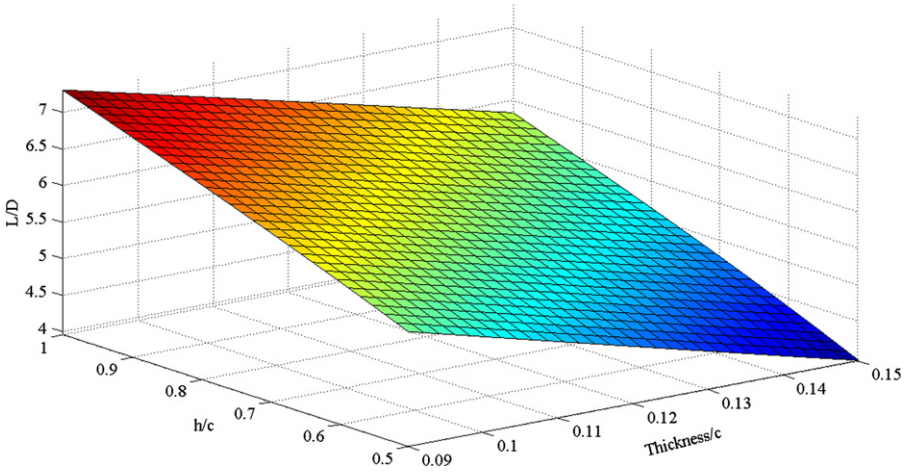

Fig. 12. Generalization of best-fitted surfaces predicted with ANFIS based thickness, h/c and L/D.

submerge hydrofoil, but they failed to give a simple mathematical model for these structures to predict the generated wave and floating hydrofoil. In this paper, a robust fuzzy knowledge based rules has been developed to predict hydrodynamic performance of a marine vehicle model and it is compared with the numerical data. Both numerical and predicted results are found to be valid within the acceptable limits. On the other hand, computer simulation on train and test data of ANFIS model demonstrates the effectiveness of the approach in terms of statistical measures, such as determination coefficient, mean square error and normalized mean-squared error. Moreover, the developed model can be used as a reference for future hydrodynamic performance studies on the marine vehicle model.

References

Antoine, D., Jacques, A.A., François, D., Jean-François, S., 2009. Computational and experimental investigation of flow over a transient pitching hydrofoil. Eur. J. Mech. B/Fluids 28, 728–743.

Antonio, C., Daniele, D., Franco, M., 2005. Hydrofoil vibration induced by a random flow: a stochastic perturbation approach. J. Sound Vib. 283, 401–432.

Assaleh, K., 2007. Extraction of fetal electrocardiogram using adaptive neuro-fuzzy inference systems. IEEE Trans. Biomed. Eng. 54 (1), 59–68.

Bateni, S., Jeng, D., 2007. Estimation of pile group scour using adaptive neuro-fuzzy approach. Ocean Eng. 34 (8–9), 1344–1354.

Bourgoyne, D., 2003. Flow Over a Hydrofoil With Trailing Edge Vortex Shedding at High-Reynolds Number.

Chen, C.K., Liu, H., 2005. A submerged vortex lattice method for calculation of the flow around three-dimensional hydrofoil. J. Ship Mech. 9, 2.

Civicioglu, P., 2007. Using uncorrupted neighborhoods of the pixels for impulsive noise suppression with ANFIS. IEEE Trans. Image Process. 16 (3), 759–773.

Daoming, G., Jie, C., 2006. ANFIS for high-pressure waterjet cleaning prediction. Surface Coat. Technol. 201 (3–4), 1629–1634.

Daskovsky, M., 2000. The hydrofoil in surface proximity, theory and experiment. Ocean Eng. 27 (10), 1129–1159.

De Blasi, P., Di Felice, F., Lalli, F., Romano, G., 2000. Experimental study of breaking wave flow field past a submerged hydrofoil by LDV. Int. J. Offshore and Polar Eng. 10, 1053–5381.

Depari, A., Flammini, A., Marioli, D., Taroni, A., 2006. Application of an ANFIS algorithm to sensor data processing. IEEE Trans. on Instrum. Meas., 1596–1599.

Djavareshkian, M., Esmaeli, A., Zamani, A., 2010. The simulation of free surface on a immersed hydrofoil in the water. In: Proceedings of the 1st Applied Hydrodynamics Conference. Tehran, Iran.

Filippov, S., 2001. Flow past a submerged hydrofoil. Fluid Dyn. 36 (3), 489–496.

Guven, A., Azamathulla, H., Zakaria, N., 2009. Linear genetic programming for prediction of circular pile scour. Ocean Eng. 36 (12–13), 985–991.

Hay, A., Visonneau, M., 2005. Computation of free-surface flows with local mesh adaptation. Int. J. Numer. Methods Fluids 49 (7), 785–816.

Huang, M., Chen, H., Huang, J., 2007. Glaucoma detection using adaptive neuro-fuzzy inference system. Expert Syst. Appl. 32 (2), 458–468.

Jang, J., 1993. ANFIS: Adaptive-network-based fuzzy inference system. IEEE Trans. Syst. Man Cybernet. 23 (3), 665–685.

Jang, J., Sun, C., Mizutani, E., 2002. Neuro-Fuzzy and Soft Computing-A Computational Approach to Learning and Machine Intelligence [Book Review]. IEEE Trans. Autom. Control 42 (10), 1482–1484.

Kazeminezhad, M., Etemad-Shahidi, A., Mousavi, S., 2005. Application of fuzzy inference system in the prediction of wave parameters. Ocean Eng. 32 (14–15), 1709–1725.

Kim, S., Yamato, H., 2005. The estimation of wave elevation and wave disturbance caused by the wave orbital motion of a fully submerged hydrofoil craft. J. Marine Sci. Technol. 10 (1), 22–31.
Kishor, N., Singh, S., Raghuvanshi, A., 2007. Adaptive intelligent hydro turbine speed identification with water and random load disturbances. Eng. Appl. Artif. Intell. 20 (6), 795–808.
Kouh, J.S., Lin, T.J., Chau, S.W., 2002. Performance an analysis of two-dimensional hydrofoil under free surface. J. Natl. Taiwan Univ. 86.
Lee, K., Gardner, P., 2006. Adaptive neuro-fuzzy inference system (ANFIS) digital predistorter for RF power amplifier linearization. IEEE Trans. Veh. Technol. 55 (1), 43–51.
Mitra, S., Hayashi, Y., 2002. Neuro-fuzzy rule generation: survey in soft computing framework. IEEE Trans. Neural Networks 11 (3), 748–768.
Noureldin, A., El-Shafie, A., Reda Taha, M., 2007. Optimizing neuro-fuzzy modules for data fusion of vehicular navigation systems using temporal cross-validation. Eng. Appl. Artif. Intell. 20 (1), 49–61.
Nuno, A.I., Arcay, B., Cotos, J.M., Varela, J., 2005. Optimization of fishing predictions by means of artificial neural networks, ANFIS, functional networks and remote sensing images. Expert Syst. Appl. 29, 356–363.
Patil, S.G., Mandal, S., Hegde, A.V., Alavandar, S. Neuro-fuzzy based approach for wave transmission prediction of horizontally interlaced multilayer moored floating pipe breakwater. Ocean Eng., in press.
Qin, H., Yang, S., 2007. Adaptive neuro-fuzzy inference systems based approach to nonlinear noise cancellation for images. Fuzzy Sets Syst. 158 (10), 1036–1063.
Rhee, S.H., Kim, S.E., Ahn, H., Oh, J., Kim, H., 2003. Analysis of a jet-controlled high-lift hydrofoil with a flap. Ocean Eng. 30, 2117–2136.
Sadathosseini, S., Mousaviraad, S., Firoozabadi, B., Ahmadi, G., 2008. Numerical simulation of free-surface waves and wave induced separation. Sci. Iran. 15 (3), 323–331.
Übeyli, E., Güler, I., 2006. Adaptive neuro-fuzzy inference system to compute quasi-TEM characteristic parameters of microshield lines with practical cavity sidewall profiles. Neurocomputing 70 (1–3), 296–304.
Xie, N., Vassalos, D., 2007. Performance analysis of 3D hydrofoil under free surface. Ocean Eng. 34 (8–9), 1257–1264.